Oyekunle and Agunbiade *J Egypt Math Soc* (2020) 28:51
https://doi.org/10.1186/s42787-020-00110-7

Journal of the Egyptian Mathematical Society

ORIGINAL RESEARCH

Open Access

Diffusion-thermo and thermal-diffusion effects with inclined magnetic field on unsteady MHD slip flow over a permeable vertical plate

T. L. Oyekunle and S. A. Agunbiade*

*Correspondence:
agunbiade1971@gmail.com
Department of Mathematics, Faculty of Physical Sciences, University of Ilorin, Ilorin, Nigeria

Abstract

In this study, various fluid physical quantities effects such as diffusion-thermo, thermal-diffusion, thermal radiation, viscous dissipation, inclined magnetic field on unsteady MHD slip flow over a permeable vertical plate are considered. The coupled and non-linear partial differential governing equations consisting of momentum, energy and species equations are reduced to ordinary differential equations using perturbation technique. The resulted coupled, nonlinear ordinary differential equations are solved by using collocation method with the aid of assumed Legendre polynomial. The impacts of different physical parameters on fluid properties are discussed and presented both graphically and tabularly. Both Dufour and Soret have the tendency of enhancing velocity profiles.

Keywords: Inclined magnetic field, Diffusion-thermo, Thermal-diffusion, MHD, Unsteady, Porous medium

Mathematics Subject Classification: 65L60, 76A05, 76M55, 76Sxx, 76W05

Introduction

In heat and mass simultaneous occurrence, it is evident that intricacy resulted due to fluxes and driving potentials relationship. Energy flux effect due to concentration gradient is referred to as diffusion-thermo (Dufour), and mass flux effect as a result of temperature gradient is known as thermal-diffusion (Soret). Most often, Dufour and Soret effects are neglected in heat and mass transfer analysis based on the assumption that they are of smaller magnitude compared to other effects as depicted by Fick's and Fourier's law. However, with reference to its applications in area like petrology, geosciences, Solar collectors, hydrology, Combustion flames, and building energy conservation, the significance of these effects become unavoidable. On this note, many researchers like Reddy et al. [1] examined Soret and Dufour effects on MHD flow via exponentially stretching sheet in the presence of viscous dissipation and thermal radiation. The result revealed that both the fluid temperature and concentration increased with a slowdown in Soret and speed-up in Dufour. Studies on effects of Soret and Dufour on Micropolar fluid were considered by Babu et al. [2]. The effects of radiation and magnetic field were

© The Author(s) 2021. **Open Access** This article is licensed under a Creative Commons Attribution 4.0 International License, which permits use, sharing, adaptation, distribution and reproduction in any medium or format, as long as you give appropriate credit to the original author(s) and the source, provide a link to the Creative Commons licence, and indicate if changes were made. The images or other third party material in this article are included in the article's Creative Commons licence, unless indicated otherwise in a credit line to the material. If material is not included in the article's Creative Commons licence and your intended use is not permitted by statutory regulation or exceeds the permitted use, you will need to obtain permission directly from the copyright holder. To view a copy of this licence, visit http://creativecommons.org/licenses/by/4.0/.

also examined. It was reported that temperature profiles declined with the increase in Soret.

Furthermore, Sekhar and Manjula [3] studied Casson fluid inclined permeable plate in the presence of Soret and Dufour with slip condition. Runge–Kutta fourth-order method was used to solve resulting ordinary differential equations. The result revealed that the increase in the angle of inclination accelerates velocity profiles. Effects of Dufour and Soret on Casson fluid were presented by Reddy and Janardhan [4]. In the study, radiation and chemical reaction effects were not given recognition. It was reported that concentration declined with the increase in Soret number. The impacts of Soret and Dufour on MHD flow with mass and heat transfer in a wavy channel were examined by Gbadeyan et al. [5]. The result showed that velocity declined with a rise in Soret, while a reverse trend is experienced for Dufour. Parandhama et al. [6] investigated effects of Soret on MHD Casson fluid via a vertical plate. The result showed that the increase in Soret decelerated temperature profiles. Salawu and Dada [7] considered pressure-driven inclined magnetic fluid flow through a Darcy Forchheimer medium in the presence of Soret and Dufour. It was reported that a rise in Soret and Dufour increases the skin friction. Iftikhar et al. [8] studied mixed convection MHD Jeffery fluid flow in the presence of Soret, Dufour and thermophoresis. The resulted partial differential equations are solved using Optimal Homotopy Analysis Method (OHAM). Convective unsteady MHD fluid flow via a permeable vertical plate with Soret and Dufour effects was carried out by Sarada and Shanker [9]. It was noticed that velocity speeds up with a rise in Dufour parameter. None of the above studies considered variable suction.

Boundary layer fluid flows in the presence of heat and mass transfer with effects of thermal radiation are applicable in numerous engineering and industrial processes such as extraction and manufacture of polymer. In addition, radiative effect has its applications in areas like cooling processes of electronic devices, nuclear reactors and technological processes involving high temperature. Navier–Stokes equations theory is basically on no-slip for the boundary conditions of the flow. But practically, it is not always applicable, especially for non-Newtonian fluid. Problems involving slip conditions and thermal radiation for various fluids have attracted the attention of researchers. Kumar [10] investigated the flow of fluid over stretched variable thickness surface of natural convective MHD Casson fluid in the presence of thermal radiation. The problem was solved numerically, and it was observed that temperature profiles are enhanced by radiation parameter. The impacts of slip conditions and radiation on stagnation point MHD flow via a stretching sheet were examined by Sumalatha et al. [11]. According to their results, the slip parameter has the tendency of declining the velocity of the fluid. Rajakumar et al. [12] presented the effects of diffusion-thermo, radiation and viscous dissipation on natural convective flow of Casson fluid over an oscillatory permeable vertical plate. Ion-slip current was put into consideration. Sreenivasulu et al. [13] considered impacts of radiation on boundary layer MHD slip flow through an exponential porous stretching sheet with dissipation and joule heating. The resulted differential equations are solved numerically with Runge–Kutta fourth-order method. The study concluded that temperature of the fluid is improved by dissipation. Agunbiade and Dada [14] discussed dissipation and chemical reaction effects on rotatory Rivlin–Ericksen fluid flow via a vertical permeable plate in the presence of thermal radiation.

In addition, Reddy and Reddy [15] examined slip boundary layer flow of convective MHD through an inclined porous surface with thermal radiation and chemical reaction. It was observed that fluid velocity tend to be higher when the angle of inclination is set to zero, while it declined with a rise in the angle of inclination. Eyring–Powell Unsteady Nanofluid flow of Hydromagnetic through a stretched inclined porous sheet in the presence of radiation and joule heating was reported by Kumar and Srinivas [16]. It is noticed that thermophoresis parameters speed up the fluid velocity. Ragavan et al. [17] examined inclined magnetic field for Walter's Liquid B fluid with entropy generation via a stretching sheet. It was reported that magnetic field strengthens with the increase in the angle of inclination. Reddy [18] discussed MHD Casson fluid flow through an inclined permeable exponentially stretching surface in the presence of chemical reaction and thermal radiation. The results revealed that inclination parameter has the tendency of enhancing velocity profiles.

This study is an extension of Sharma and Choudhary [19], and in view of the above studies, combined effects of diffusion-thermo, thermal-diffusion, viscous dissipation and thermal radiation on unsteady MHD slip flow with inclined magnetic field over a permeable vertical plate have not being given adequate attention. Practically, combined effects of these parameters are significantly important in numerous engineering and industrial processes. Therefore, this study is motivated to consider diffusion-thermo and thermal-diffusion effects on unsteady MHD slip flow with inclined magnetic field, thermal radiation, viscous dissipation and variable suction. The results of the coupled nonlinear differential equations governing the flow were obtained using collocation method with the aid of assumed Legendre polynomial.

Main text

Consider unsteady free convective MHD laminar incompressible, electrically conducting fluid flow via a permeable medium with slip condition in the presence of inclined magnetic field, diffusion-thermo and thermal-diffusion. The plate is considered to be porous and infinite, x-axis is considered in the vertical direction of the plate, while η-axis is perpendicular to the plate. There is application of inclined magnetic field in η-axis direction. Soret and Dufour are not negligible because it is assumed to be of substantial magnitude. Since application of voltage externally is absent, electric field is not considered. The flow configuration is shown below (Fig. 1).

Based on Boussinesq approximation and the above assumptions, the equations governing the flow can be expressed as

$$\frac{\partial v^*}{\partial \eta^*} = 0 \tag{1}$$

$$\frac{\partial h^*}{\partial t^*} - V^*\frac{\partial h^*}{\partial \eta^*} = \frac{\partial H^*_\infty}{\partial t^*} + g\beta\left(\vartheta^* - \vartheta_\infty\right) - g\beta^*\left(\zeta^* - \zeta_\infty\right) + \nu\frac{\partial^2 h^*}{\partial \eta^{*2}} - \left(\frac{\nu}{K^*} + B\sin^2\psi\right)\left(h^* - H^*_\infty\right) \tag{2}$$

$$\frac{\partial \vartheta^*}{\partial t^*} - V^*\frac{\partial \vartheta^*}{\partial \eta^*} = \frac{k}{\rho C_\mathrm{p}}\left(\frac{\partial^2 \vartheta^*}{\partial \eta^{*2}} - \frac{1}{k}\frac{\partial q_r^*}{\partial \eta^*}\right) + \frac{\mu}{\rho C_\mathrm{p}}\left(\frac{\partial h^*}{\partial \eta^*}\right)^2 + \frac{DK_\vartheta}{C_\mathrm{p} C_\mathrm{s}}\frac{\partial^2 \zeta^*}{\partial \eta^{*2}} \tag{3}$$

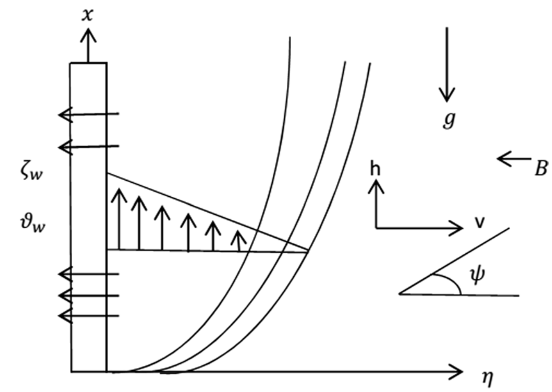

Fig. 1 Geometry of the problem

$$\frac{\partial \zeta^*}{\partial t^*} - V^* \frac{\partial \zeta^*}{\partial \eta^*} = D \frac{\partial^2 \zeta^*}{\partial \eta^{*2}} - k_1^* (\zeta^* - \zeta_\infty) + \frac{D K_\vartheta}{\vartheta_m} \frac{\partial^2 \vartheta^*}{\partial \eta^{*2}} \tag{4}$$

where h^* and v^* are dimensional velocity components in x^* and η^* directions, respectively, t^* is the dimensional time, V^* is the constant suction velocity, H_∞^* is the free stream velocity, g is the acceleration as a result of gravitational force, β is the thermal expansion coefficient, β^* concentration expansion coefficient, ϑ^* is the dimensional temperature, ϑ_∞ is the temperature of the fluid at the free stream, ζ^* is the boundary layer species concentration, ζ_∞ is the species concentration at the free stream, ν is the kinematic viscosity, K^* is the permeability of porous medium, B is the magnetic field intensity, ψ is the angle of inclination of magnetic field, k is the thermal conductivity,C_p is the specific heat at constant pressure, q_r^* is the radiation heat flux, ρ is the fluid density, μ is the viscosity coefficient, D is the mass diffusivity, K_ϑ is the thermal diffusion ratio, C_s concentration susceptibility, k_1^* is the chemical reaction coefficient, and ϑ_m is the mean fluid temperature.

The boundary conditions are:

$$\left.\begin{array}{ll} h^* = S^*\left(\frac{\partial h^*}{\partial \eta^*}\right), \vartheta^* = \vartheta_w + \varepsilon(\vartheta_w - \vartheta_\infty)e^{i\omega^* t^*}, \zeta^* = \zeta_w + \varepsilon(\zeta_w - \zeta_\infty)e^{i\omega^* t^*} & \text{at } \eta^* = 0; \\ h^* \to H_\infty(t^*) = H_0\left(1 + \varepsilon A e^{i\omega^* t^*}\right), \vartheta^* \to \vartheta_\infty, \zeta^* \to \zeta_\infty & \text{at } \eta^* = \infty \end{array}\right\} \tag{5}$$

Here ε is the scalar constant, A is the non-dimensional suction velocity parameter, ω^* is the dimensional oscillation parameter, S^* is the slip parameter, ϑ_w and ζ_w are the temperature and species concentration at the plate, respectively, H_∞ is the free stream velocity, and H_0 is a constant. The suction velocity is normal to the plate and is expressed as a function of time in the form

$$V^* = -V_0\left(1 + \varepsilon A e^{i\omega^* t^*}\right) \tag{6}$$

Radiative heat flux is given as

$$q_r^* = -\frac{4\sigma_s}{3k_e} \frac{\partial \vartheta^{*4}}{\partial \eta^*} \tag{7}$$

Expanding ϑ^{*4} using Taylor series expansion and ignoring higher order terms from second order gives

$$\vartheta^{*4} = 4\vartheta_{\infty}^{*3}\vartheta^{*} - 3\vartheta_{\infty}^{*4} \tag{8}$$

Method of solution

The following non-dimensional quantities

$$\left.\begin{array}{l} h = \frac{h^*}{V_0}, \eta = \frac{V_0\eta^*}{\nu}, \xi = \frac{\vartheta^* - \vartheta_\infty}{\vartheta_{\mathrm{w}} - \vartheta_\infty}, \zeta = \frac{\zeta^* - \zeta_\infty}{\zeta_{\mathrm{w}} - \zeta_\infty}, t = \frac{t^* V_0^2}{4\nu}, \omega = \frac{4\omega^*\nu}{V_0^2}, D_{\mathrm{u}} = \frac{DK_\vartheta(\zeta_{\mathrm{w}}^* - \zeta_\infty)}{C_{\mathrm{s}}C_{\mathrm{p}}\nu(\vartheta_{\mathrm{w}}^* - \vartheta_\infty)} \\ S_t = \frac{DK_\vartheta(\vartheta_{\mathrm{w}}^* - \vartheta_\infty)}{\nu\vartheta_{\mathrm{m}}(\zeta_{\mathrm{w}}^* - \zeta_\infty)}, H_g = \frac{\nu g\beta(\vartheta_{\mathrm{w}} - \vartheta_\infty)}{V_0^3}, M_{\mathrm{g}} = \frac{\nu g\beta^*(\zeta_{\mathrm{w}} - \zeta_\infty)}{V_0^3}, M = \frac{B\nu}{V_0^2}, P_{\mathrm{r}} = \frac{\mu C_p}{k}, \\ K = \frac{K^* V_0^2}{\nu^2}, R_{\mathrm{d}} = \frac{k_e K}{4\sigma_{\mathrm{s}}\vartheta_\infty^3}, E_{\mathrm{c}} = \frac{V_0^2}{C_p(\vartheta_{\mathrm{w}}^* - \vartheta_\infty)}, S_{\mathrm{c}} = \frac{\nu}{D}, H = \frac{H_\infty^*}{V_0}, S = \frac{V_0 S^*}{\nu}, k_1 = \frac{\nu k_1^*}{V_0^2}, \nu = \frac{\nu^*}{V_0} \end{array}\right\} \tag{9}$$

Equations (10)–(13) are obtained by introducing Eqs. (6)–(9) to Eqs. (2)–(5)

$$\frac{1}{4}\frac{\partial h}{\partial t} - \left(1 + \varepsilon A e^{i\omega t}\right)\frac{\partial h}{\partial \eta} = \frac{1}{4}\frac{\partial H}{\partial t} + \frac{\partial^2 h}{\partial \eta^2} + H_{\mathrm{g}}\xi + M_{\mathrm{g}}\zeta - \left(M\sin^2\psi + \frac{1}{K}\right)(h - H) \tag{10}$$

$$\frac{1}{4}\frac{\partial \xi}{\partial t} - \left(1 + \varepsilon A e^{i\omega t}\right)\frac{\partial \xi}{\partial \eta} = \frac{1}{P_{\mathrm{r}}}\left(1 + \frac{4}{3R_{\mathrm{d}}}\right)\frac{\partial^2 \xi}{\partial \eta^2} + E_{\mathrm{c}}\left(\frac{\partial h}{\partial \eta}\right)^2 + D_{\mathrm{u}}\frac{\partial^2 \zeta}{\partial \eta^2} \tag{11}$$

$$\frac{1}{4}\frac{\partial \zeta}{\partial t} - \left(1 + \varepsilon A e^{i\omega t}\right)\frac{\partial \zeta}{\partial \eta} = \frac{1}{S_{\mathrm{c}}}\frac{\partial^2 \zeta}{\partial \eta^2} - k_1\zeta + S_{\mathrm{t}}\frac{\partial^2 \xi}{\partial \eta^2} \tag{12}$$

The boundary in non-dimensional form is

$$\left.\begin{array}{ll} h = S\left(\frac{\partial h}{\partial \eta}\right), \xi = 1 + \varepsilon e^{i\omega t}, \zeta = 1 + \varepsilon e^{i\omega t} & \text{at } \eta = 0; \\ h \to \lambda\left(1 + \varepsilon A e^{i\omega t}\right), \xi \to 0, \zeta \to 0 & \text{at } \eta \to \infty \end{array}\right\} \tag{13}$$

where S is the slip parameter, $\lambda = \frac{H_0}{V_0}$, h is the non-dimensional velocity along x-axis, ξ is the non-dimensional fluid temperature, ζ is the non-dimensional concentration, D_{u} is the Dufour parameter, S_{t} is the Soret parameter, H_{g} and M_{g} are the Grashof number for heat and mass transfer, respectively, M is the Hartmann number, P_{r} is the Prandtl number, K is the permeability parameter, R_{d} is the radiation parameter, E_{c} is the Eckert number, S_{c} is the Schmidt number, H is the free stream velocity, k_1 is the chemical reaction parameter, σ_s is the fluid electrical conductivity, and k_{e} is the mean absorption coefficient.

Considering the associated boundary conditions, the assumed solutions can be expressed as

$$\left.\begin{array}{l} h(\eta, t) = h_0(\eta) + \varepsilon e^{i\omega t} h_1(\eta) \\ \xi(\eta, t) = \xi_0(\eta) + \varepsilon e^{i\omega t}\xi_1(\eta) \\ \zeta(\eta, t) = \zeta_0(\eta) + \varepsilon e^{i\omega t}\zeta_1(\eta) \end{array}\right\} \tag{14}$$

Applying assumed solutions (14) to Eqs. (10)–(13) and equating the terms, harmonic and non-harmonic, gives

$$h_0'' + h_0' - \left(M\sin^2\psi + \frac{1}{K}\right)h_0 = -H_g\xi_0 - M_g\zeta_0 - \left(M\sin^2\psi + \frac{1}{K}\right)\lambda \tag{15}$$

$$h_1'' + h_1' - \left(M\sin^2\psi + \frac{1}{K}\right)h_1 = -H_g\xi_1 - M_g\zeta_1 - \left(M\sin^2\psi + \frac{1}{K}\right)A\lambda \tag{16}$$

$$\xi_0'' + P_r\left(1 + \frac{4}{3R_d}\right)^{-1}\xi_0' = E_cP_r\left(1 + \frac{4}{3R_d}\right)^{-1}h_0'^2 - D_u\zeta_0'' \tag{17}$$

$$\begin{aligned} &\xi_1'' + P_r\left(1 + \frac{4}{3R_d}\right)^{-1}\xi_1' - \frac{i\omega P_r}{4}\left(1 + \frac{4}{3R_d}\right)^{-1}\xi_1 \\ &\quad = -AP_r\left(1 + \frac{4}{3R_d}\right)^{-1}\xi_0' - 2E_cP_r\left(1 + \frac{4}{3R_d}\right)^{-1}h_0'h_1' - D_u\zeta_1'' \end{aligned} \tag{18}$$

$$\zeta_0'' + S_c\zeta_0' - k_1S_c\zeta_0 = -S_t\xi_0'' \tag{19}$$

$$\zeta_1'' + S_c\zeta_1' - S_c\left(\frac{i\omega}{4} + k_1\right)\zeta_1 = -S_cA\zeta_0' - S_t\xi_1'' \tag{20}$$

Now, the boundary conditions reduced to

$$\left.\begin{aligned} &h_0 = S\left(\tfrac{\partial h_0}{\partial \eta}\right), h_1 = S\left(\tfrac{\partial h_1}{\partial \eta}\right), \xi_0 = 1, \xi_1 = 1\zeta_0 = 1\zeta_1 = 1 \;\text{ at } \eta = 0; \\ &h_0 \to \lambda, h_1 \to A\lambda, \xi_0 \to 0, \xi_1 \to 0, \zeta_0 \to 0\zeta_1 \to 0 \qquad \text{at } \eta \to \infty \end{aligned}\right\} \tag{21}$$

Legendre collocation method

The solutions to the coupled, nonlinear ordinary differential Eqs. (15)–(20) with the boundary conditions (21) are obtained using collocation method with assumed Legendre polynomial. Applying the domain truncation method, the interval $[0,\infty)$ is transformed to $[0,L]$. The Legendre polynomial is of interval $[-1,1]$ which is transformed to $[0,L]$ using the transformation

$$y = \frac{2\eta}{L} - 1. \tag{22}$$

Hence, the boundary value problem is solved within the region $[0,L]$ instead of $[0,\infty)$, where L (scaling parameter) is taken to be sufficiently large enough to take care of the thickness of the boundary layer (Olagunju et al. [20] and Aysun and Salih [21]).

Therefore, the Legendre polynomial is expressed as

$$h_0 = \sum_{j=0}^{N} a_jP_j(y) \quad \text{for } j = 0, 1, 2, 3, 4, \ldots, N \tag{23}$$

Hence,

$$h_0 = a_0 P_0(y) + a_1 P_1(y) + a_2 P_2(y) + \cdots \tag{24}$$

where

$$P_0(y) = 1, \quad P_1(y) = y, \quad P_2(y) = \frac{1}{2}\left(3y^2 - 1\right) \tag{25}$$

Substituting Eqs. (22) and (25) in Eq. (24) gives

$$h_0 = a_0 + a_1\left(2\frac{\eta}{L} - 1\right) + \frac{a_2}{2}\left[3\left(2\frac{\eta}{L} - 1\right)^2 - 1\right] + \cdots \tag{26}$$

For $L = 20$ and $N = 20$, Eq. (26) becomes

$$h_0 = a_0 + \frac{1}{10}(-10 + \eta)a_1 + \frac{1}{200}\left(200 - 60\eta + 3\eta^2\right)a_2 + \cdots \tag{27}$$

Similarly,

$$h_1 = b_0 + \frac{1}{10}(-10 + \eta)b_1 + \frac{1}{200}\left(200 - 60\eta + 3\eta^2\right)b_2 + \cdots \tag{28}$$

$$\xi_0 = c_0 + \frac{1}{10}(-10 + \eta)c_1 + \frac{1}{200}\left(200 - 60\eta + 3\eta^2\right)c_2 + \cdots \tag{29}$$

$$\xi_1 = d_0 + \frac{1}{10}(-10 + \eta)d_1 + \frac{1}{200}\left(200 - 60\eta + 3\eta^2\right)d_2 + \cdots \tag{30}$$

$$\zeta_0 = e_0 + \frac{1}{10}(-10 + \eta)e_1 + \frac{1}{200}\left(200 - 60\eta + 3\eta^2\right)e_2 + \cdots \tag{31}$$

$$\zeta_1 = f_0 + \frac{1}{10}(-10 + \eta)f_1 + \frac{1}{200}\left(200 - 60\eta + 3\eta^2\right)f_2 + \cdots \tag{32}$$

$\{a_0, a_1, \ldots, a_N\}$, $\left\{b_0, b_1, \ldots, b_N\right\}$, $\{c_0, c_1, \ldots, c_N\}$, $\left\{d_0, d_1, \ldots, d_N\right\}$, $\{e_0, e, \ldots, e_N\}$ and $\left\{f_0, f, \ldots, f_N\right\}$ are unknown coefficients which can be obtained using the coupled, nonlinear differential Eqs. (15)–(20) with the boundary conditions (21). Hence, the approximate solutions of the truncated series (27)–(32) can be obtained.

$$\text{Collpoints} = \text{NSolve}\left[\text{Expand}\left[\text{LegendreP}\left[N - 1, 2\frac{\eta}{L} - 1\right]\right] = 0, \eta\right] \tag{33}$$

Equation (33) is a MATHEMATICA Software Language used to generate the following collocation points for values of η.

$$\left.\begin{array}{l} 0.0759316,\quad 0.397918,\quad 0.968441,\quad 1.77285,\quad 2.79034,\quad 3.99455,\\ 5.35429,\quad 6.83436,\quad 8.39641,\quad 10.0000,\quad 11.6036,\quad 13.1657,\\ 14.646,\quad 16.0051,\quad 17.2097,\quad 18.2273,\quad 19.0319,\quad 19.6002,\quad 19.9241 \end{array}\right\} \tag{34}$$

Equations (27)–(32) are substituted in Eqs. (15)–(20), with the default values for the fluid parameters; $H_g = 5,\ M_g = 5,\ P_r = 0.71,\ E_c = 0.01,\ \psi = \frac{\pi}{2},\ k_1 = 0.1,\ S_c = 0.22,$

$R_d = 1.6$, $K = 0.1$, $D_u = 0.1$, $S_t = 0.2$, $M = 1$, $t = 0.1$, $A = 0.5$, $S = 0.2$, $\lambda = 0.5$, $\omega = 1$, and $\varepsilon = 0.1$, to give six residual equations. By imposing the boundary conditions (21) on Eqs. (27)–(32), twelve equations are derived. Each residual equation is collocated at the above collocation points to yield one hundred and fourteen collocation equations. Consequently, there are a total number of one hundred and twenty-six equations with one hundred and twenty-six unknown coefficients. These equations are solved using MATHEMATICA 11.0 software. The numerical values obtained for the unknown coefficients are then substituted back into Eqs. (27)–(32). Hence, Eq. (14) becomes

$$\begin{aligned} h = {} & 0.631525 + 5.71453 \times 10^{-25} i - \left(0.0248978 + 3.12151 \times 10^{-25} i\right)(-10 + \eta) \\ & + \left(0.000790613 + 7.21393 \times 10^{-27} i\right)\left(200 - 60\eta + 3\eta^2\right) \\ & - \left(0.0000480709 - 8.45787 \times 10^{-27} i\right)\left(-400 + 240\eta - 30\eta^2 + \eta^3\right) - \end{aligned} \tag{35}$$

$$\begin{aligned} \xi = {} & 0.140729 + 1.49935 \times 10^{-24} i - (0.030269 + 7.79491 \times 10^{-25} i) - 10 + \eta \\ & + (0.00136063 + 1.65512 \times 10^{-26} i)(200 - 60\eta + 3\eta^2) \\ & - (0.0041331 - 2.16109 \times 10^{-26} i)(-400 + 240\eta - 30\eta^2 + \eta^3) + \ldots \end{aligned} \tag{36}$$

$$\begin{aligned} \zeta = {} & 0.194627 - 2.1262 \times 10^{-25} i - (00373656 - 8.6365 \times 10^{-26} i)(-10 + \eta) \\ & + (0.00134708 - 1.58859 \times 10^{-27} i)(200 - 60\eta + 3\eta^2) \\ & (0.000299884 + 2.32537 \times 10^{-27} i)(-400 + 240\eta - 30\eta^2 + \eta^3) + \ldots \end{aligned} \tag{37}$$

Skin-friction:

The coefficient of skin-friction in non-dimensional form is expressed as

$$C_f = \left(\frac{\partial}{\partial \eta}\left(h_0(\eta) + \varepsilon e^{i\omega t} h_1(\eta)\right)\right)_{\eta=0} \tag{38}$$

Nusselt Number

The rate of heat transfer at the plate is expressed as

$$\mathrm{Nu} = -\left(\frac{\partial}{\partial \eta}\left(\xi_0(\eta) + \varepsilon e^{i\omega t} \xi_1(\eta)\right)\right)_{\eta=0} \tag{39}$$

Sherwood Number

The rate of mass transfer in non-dimensional form is given as

$$\mathrm{Sh} = -\left(\frac{\partial}{\partial \eta}\left(\zeta_0(\eta) + \varepsilon e^{i\omega t} \zeta_1(\eta)\right)\right)_{\eta=0} \tag{40}$$

Results and discussion

Ordinary differential Eqs. (15)–(20) with the boundary conditions (21) are solved using collocation method with the aid of assumed Legendre polynomial. On velocity, temperature and concentration profiles, the impacts of various parameters are considered and

Table 1 Comparison of the present work with Sharma and Choudhary [19]

	Sharma and Choudhary		Present work	
R	**Temp. (ξ)**	**Conc. (ζ)**	**Temp. (ξ)**	**Conc. (ζ)**
1.0	0.3062	0.2978	0.2999	0.2988
1.6	0.3895	0.2978	0.3812	0.2988
k_1	**Temp. (ξ)**	**Conc. (ζ)**	**Temp. (ξ)**	**Conc. (ζ)**
0.1	0.3895	0.2978	0.3812	0.2988
0.4	0.3897	0.4307	0.3816	0.4314

Table 2 Comparison of the collocation method with fourth-order Runge–Kutta method

D_u	S_t	E_c	k_1	R_d	Collocation method	4th order R-K	$\|d\|$
0.3					5.10354	5.10354	0.00000
0.6					5.13080	5.13080	0.00000
	0.2				5.08704	5.08704	0.00000
	0.6				5.14038	5.14038	0.00000
		0.05			5.09275	5.09272	0.00003
		0.07			5.09561	5.09557	0.00004
			0.3		5.04433	5.04432	0.00001
			0.7		4.98716	4.98715	0.00001
				0.7	5.13774	5.13773	0.00001
				1.7	5.08322	5.08321	0.00001

the results are presented both in graphical and tabular forms. For the computations, the default values are: $H_g = 5$, $M_g = 5$, $P_r = 0.71$, $E_c = 0.01$, $\psi = \frac{\pi}{2}$, $k_1 = 0.1$, $S_c = 0.22$, $R_d = 1.6$, $K = 0.1$, $D_u = 0.1$, $S_t = 0.2$, $M = 1$, $t = 0.1$, $A = 0.5$, $S = 0.2$, $\lambda = 0.5$, $\omega = 1$, and $\varepsilon = 0.1$. The comparison of this work with the work of Sharma and Choudhary [19] is presented in Table 1, by setting Dufour and Soret parameters to zero, an excellent agreement is observed. In order to further validate the results, the comparison of Legendre collocation method with fourth-order Runge–Kutta method for skin friction, Nusselt number and Sherwood Number is displayed in Table 2 where d is the difference between the collocation method and fourth-order R-K.

Figures 2 and 3 display the variation of thermal H_g and solutal M_g Grashof number, respectively, on velocity profiles. Physically, increase in thermal Grashof number will make the buoyancy force to rise, which in turn accelerates within the channel the viscous hydrodynamics. Solutal Grashof number can be expressed as ratio of concentration buoyancy force to viscous hydrodynamic force. From these figures, it is obvious that a rise in H_g enhanced velocity profiles. The same trend is evidence in Fig. 3, a hike in M_g speed-up velocity profiles.

Effects of angle of inclination parameter ψ is depicted in Fig. 4. Increase in ψ retards the velocity distribution. This is as a result of magnetic field being strengthen with a rise in ψ. Magnetic field exhibits a resistance force known as Lorentz force. This force resists the fluid motion. Hence, in Fig. 5 it is evident that Hartmann number M has the tendency of retarding the fluid velocity.

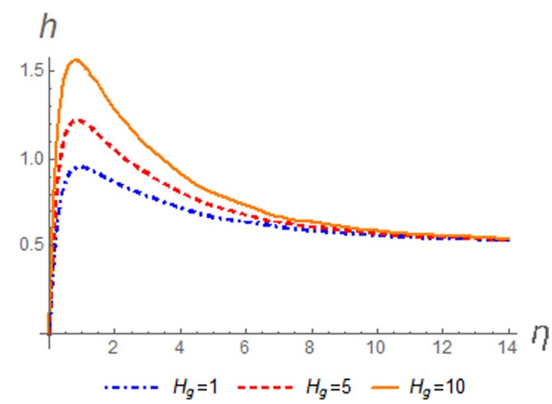

Fig. 2 Effect of H_g on the velocity profile

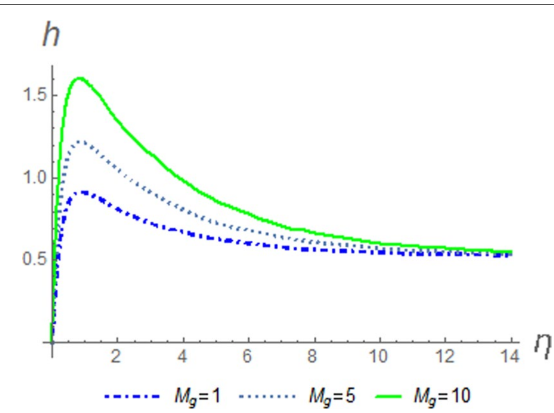

Fig. 3 Effect of M_g on the velocity profile

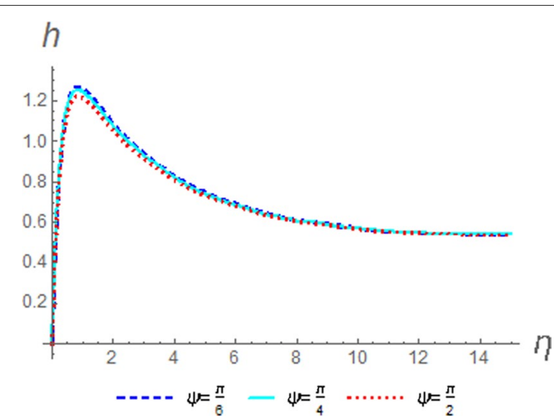

Fig. 4 Effect of ψ on the velocity profile

Figure 6 portrays effects of permeability of the porous medium parameter (K) on velocity profiles. Momentum boundary layer thickness is boosted with higher values of K. Physically, this result can be justified by ignoring the permeability holes.

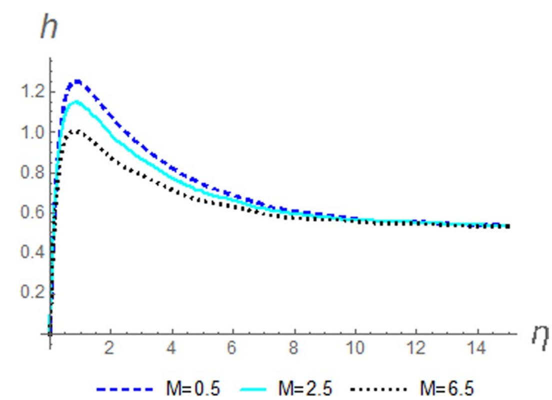

Fig. 5 Effect of *M* on the velocity profile

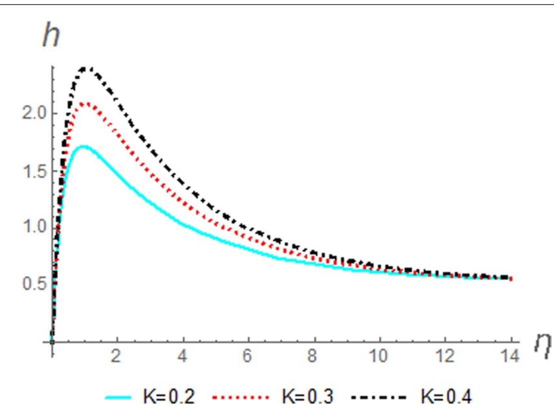

Fig. 6 Effect of *K* on the velocity profile

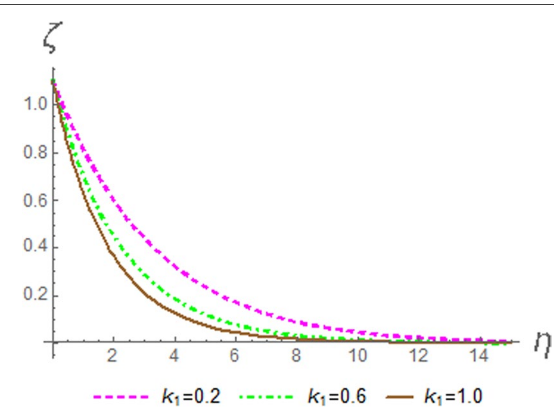

Fig. 7 Effect of k_1 on the concentration profile

Variation of chemical reaction parameter (k_1) on concentration and velocity distribution is detected in Figs. 7 and 8. It is observed in Fig. 7 that a hike in the value of k_1 slowed down the concentration profiles. This is as a result of reduction in solutal boundary layer thickness and mass transfer increases due to destructive chemical.

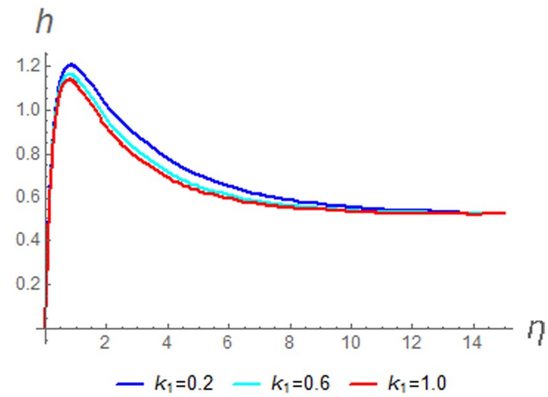

Fig. 8 Effect of k_1 on the velocity profile

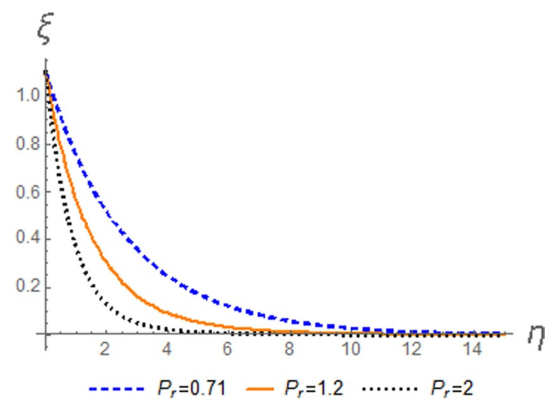

Fig. 9 Effect of P_r on the temperature profile

The same trend is apparent in Fig. 8; k_1 has the tendency of retarding the velocity of the fluid.

The effects of Prandtl number (P_r) on temperature and velocity profile are elucidated in Figs. 9 and 10. Prandtl can be expressed as relativity of momentum diffusivity to thermal diffusivity; therefore, high thermal conductivity reduced the velocity of the fluid. High values of P_r imply high thermal conductivity; hence from the heated surface, heat diffuses away more rapidly. Consequently, the thermal boundary layer is lessened with hike in P_r, as displayed in Fig. 10.

Figures 11 and 12 show the variation of thermal radiation (R_d) on temperature and velocity profiles. Dominance of conduction over R_d accelerated with a rise in thermal radiation. As a result, both buoyancy force and thermal boundary temperature are slowed down. Generally, though trivial fact, there is inverse proportionality between thermal radiation and temperature. From Fig. 12, it is noticed that the increase in R_d decelerated the velocity distributions.

It is shown in Figs. 13 and 14 the effects of Schmidt number (S_c) on concentration and velocity distribution. Both concentration and velocity are retarded with the increase in S_c. Physically, a boost in S_c implies a reverse trend in molecular diffusion.

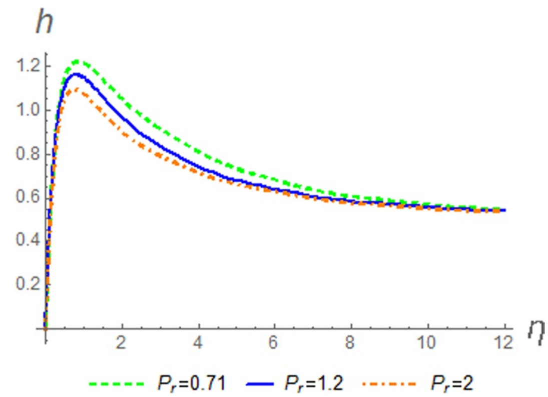

Fig. 10 Effect of P_r on the velocity profile

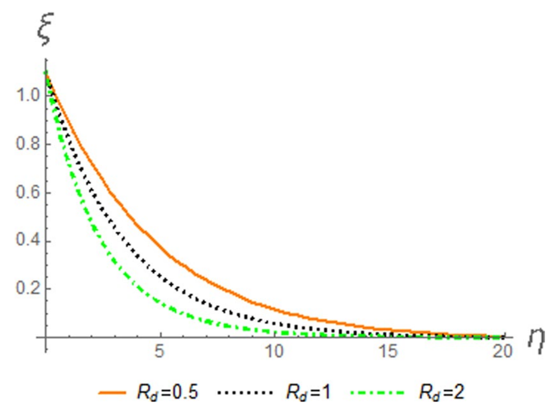

Fig. 11 Effect of R_d on the temperature profile

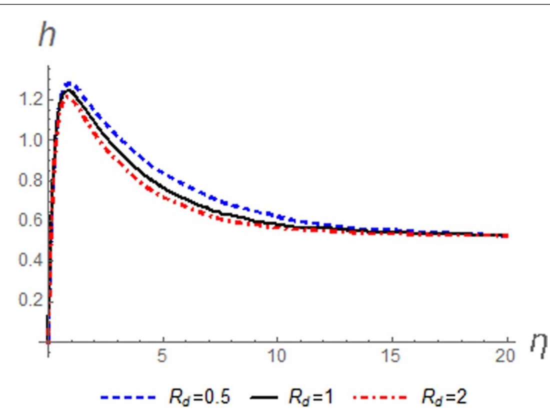

Fig. 12 Effect of R_d on the velocity profile

Figures 15, 16 and 17 reveal the effects of thermal-diffusion (S_t) on concentration, temperature and velocity distributions. A careful examination of these figures shows that concentration and velocity improved for higher values of S_t. Soret (S_t) resulted

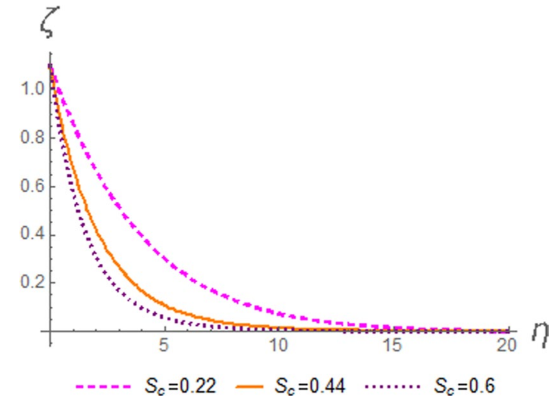

Fig. 13 Effect of S_c on the concentration profile

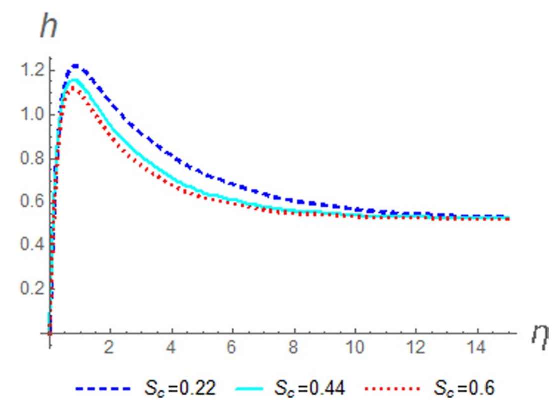

Fig. 14 Effect of S_c on the velocity profile

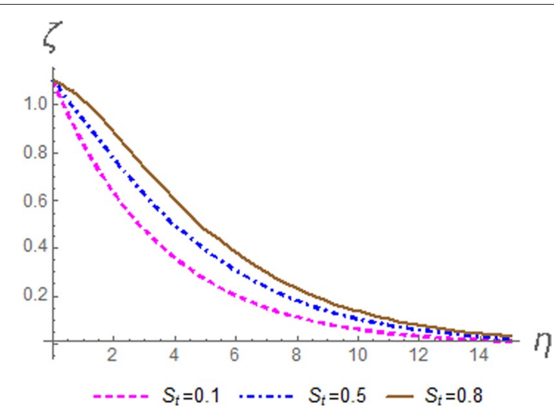

Fig. 15 Effect of S_t on the concentration profile

from mass flux; hence, there is tendency for concentration to increase. In Fig. 16, the effect of S_t on the temperature of the fluid is not noticeable. Figures 18, 19 and 20 depict the variation of diffusion-thermo (D_u) on concentration, temperature and

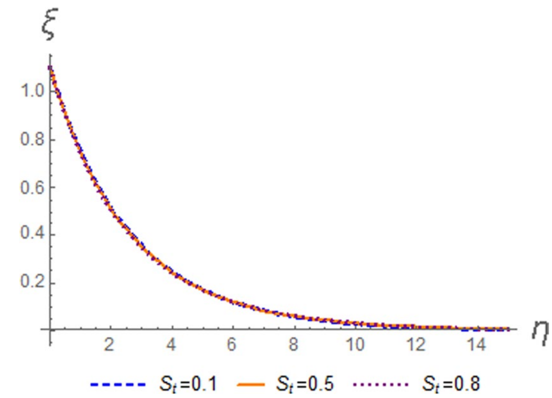

Fig. 16 Effect of S_t on the temperature profile

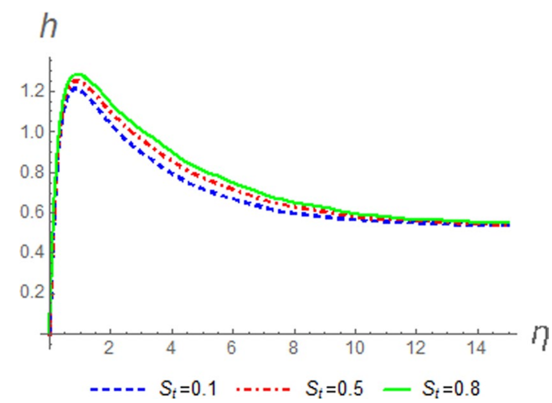

Fig. 17 Effect of S_t on the velocity profile

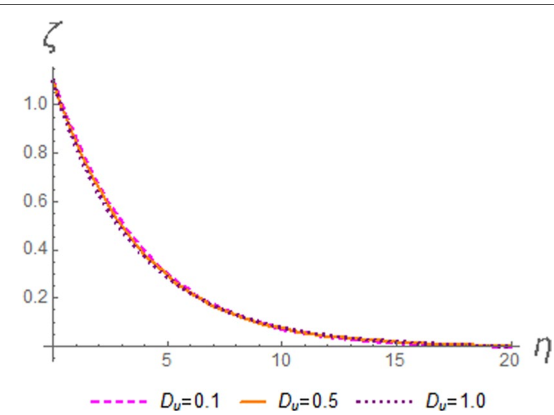

Fig. 18 Effect of D_u on the concentration profile

velocity. Both temperature and velocity accelerated as the values of D_u speed up. The enhancement of temperature due to a rise in D_u is as a result of energy flux being

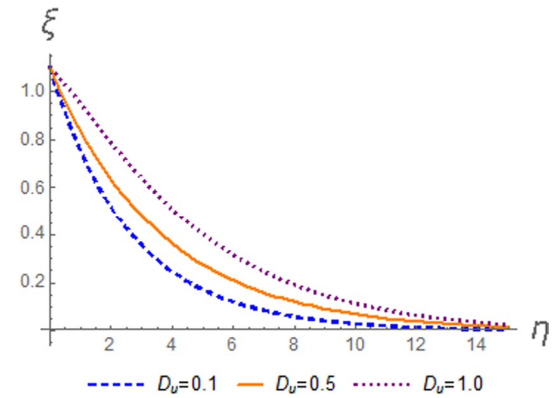

Fig. 19 Effect of D_u on the temperature profile

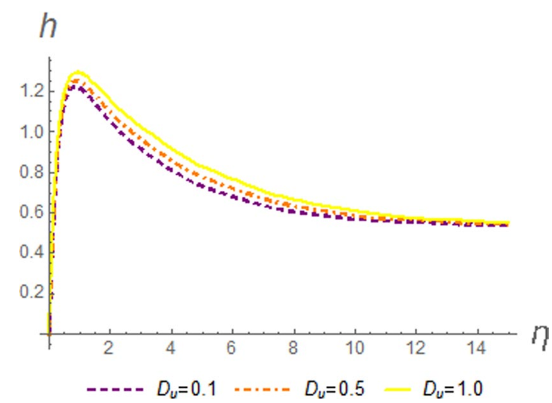

Fig. 20 Effect of D_u on the velocity profile

Table 3 Effect of Soret (S_t) on the concentration profile

η	**0**	**2**	**4**	**6**	**8**	**10**	**12**
$S_t = 0.1$	1.099500	0.632188	0.358456	0.201081	0.111797	0.061527	0.033302
$S_t = 0.5$	1.099500	0.774195	0.497873	0.304587	0.180726	0.104751	0.059191
$S_t = 0.8$	1.099500	0.884066	0.602424	0.380692	0.230938	0.136207	0.078126

η	**14**	**16**	**18**	**20**
$S_t = 0.1$	0.017421	0.008389	0.003151	2.663072×10^{-17}
$S_t = 0.5$	0.032146	0.015973	0.006158	$-3.840786 \times 10^{-17}$
$S_t = 0.8$	0.043017	0.021637	0.008431	$-1.832301 \times 10^{-17}$

generated. Consequently, there is increase in heat of the fluid flow. It is apparent in Fig. 18 that concentration profiles are indifference to the increase in D_u.

Tables 3, 4 and 5 are the numerical presentation of Figs. 15, 16 and 17, respectively. In Table 4, there is evidence of slight impact of Soret on the fluid temperature, though this effect is not noticeable on the graph. It is obvious in Table 4 that from $\eta = 0$ to

Table 4 Effect of Soret (S_t) on the temperature profile

η	0	2	4	6	8	10	12
$S_t = 0.1$	1.099500	0.518484	0.247139		0.058668	0.029054	0.014355
$S_t = 0.5$	1.099500	0.509459	0.243169	0.119894	0.060664	0.031242	0.016106
$S_t = 0.8$	1.099500	0.502553	0.240365	0.120271	0.062239	0.032888	0.017395

η	14	16	18	20
$S_t = 0.1$	0.006846	0.003030	0.001044	8.361909×10^{-18}
$S_t = 0.5$	0.008017	0.003691	0.001318	$-1.928525 \times 10^{-17}$
$S_t = 0.8$	0.008867	0.004169	0.001514	$-1.324082 \times 10^{-17}$

Table 5 Effect of Soret (S_t) on the velocity profile

η	0	2	4	6	8	10
$S_t = 0.1$	1.110223×10^{-16}	1.034678	0.794341	0.670473	0.599357	0.565011
$S_t = 0.5$	1.110223×10^{-16}	1.094751	0.855088	0.716909	0.631038	0.585281
$S_t = 0.8$	2.220446×10^{-16}	1.141179	0.900692	0.751129	0.654171	0.600058

η	12	14	16	18	20
$S_t = 0.1$	0.547432	0.534347	0.529838	0.527093	0.524875
$S_t = 0.5$	0.559761	0.541413	0.533488	0.528522	0.524875
$S_t = 0.8$	0.568785	0.546624	0.536206	0.529597	0.524875

$\eta = 4$, temperature tends to decline, while a different trend is observed from $\eta = 6$ to $\eta = 20$ where Soret (S_t) shows the tendency of enhancing the fluid temperature.

Table 6 displays the effects of E_c, R, k_1, ψ, S_t and D_u on Skin-friction C_f, Nusselt number Nu and Sherwood Number Sh. It is discovered that E_c, S_t and D_u have the tendency of enhancing C_f, while it is slowed down by R, k_1 and ψ. The heat transfer is improved with the increase in R, ψ and S_t. A reverse trend is noticed for a rise in E_c, k_1 and D_u. Finally, mass transfer accelerated as a result of a hike in E_c, k_1 and D_u. On the other hand, Sh is lessened with the increase in R, ψ and S_t.

Conclusion

This study is carried out to examine the combined effects of diffusion-thermo, thermal-diffusion, viscous dissipation and thermal radiation on unsteady MHD slip flow with inclined magnetic field over a permeable vertical plate. The nonlinear coupled differential equations are solved using collocation method with the aid of assumed Legendre polynomial. The results are graphically and tabularly presented. From the study, though Dufour and Soret has the tendency of improving the fluid velocity but mass flux as a result of temperature gradient has insignificant impact on temperature of the fluid, likewise energy flux on concentration. The result revealed that Soret and Dufour effect is relevant in mixture of gases of light molecular weight and is applicable in different areas.

It is detected that:

(i) Velocity of the fluid is retarded with a rise in ψ, M, k_1, P_r, R_d, and S_c. On the other hand, the fluid velocity improved for higher values of H_g, M_g, K, S_t and D_u.

(ii) Increase in P_r and R_d reduced the thermal boundary layer.

Table 6 Values of skin-friction, Nusselt number and Sherwood Number for different parameters

R_d	E_c	k_1	ψ	S_t	D_u	C_f	Nu	Sh
0.5						5.58856	0.19238	0.30835
1.0						5.53619	0.31281	0.28514
1.5						5.50341	0.39306	0.26950
	0.02					5.49998	0.39145	0.26987
	0.03					5.50165	0.37699	0.27276
	0.04					5.50332	0.36251	0.27565
		0.2				5.46935	0.39956	0.33086
		0.4				5.42733	0.39012	0.42709
		0.6				5.39572	0.38276	0.50258
			$\frac{\pi}{6}$			5.56836	0.40512	0.26714
			$\frac{\pi}{5}$			5.55877	0.40523	0.26712
			$\frac{\pi}{4}$			5.54367	0.40539	0.26709
				0.1		5.48278	0.40254	0.30093
				0.4		5.53015	0.41279	0.19703
				0.7		5.57999	0.42367	0.08659
					0.2	5.50922	0.37886	0.27225
					0.5	5.54415	0.29078	0.28942
					0.8	5.58280	0.19053	0.30902

(iii) The concentration profiles are improved for higher values of S_t, while they decelerated with hike in k_1.

Abbreviation
MHD: Magneto-hydrodynamic.

Acknowledgements
Authors express their sincere gratitude to the reviewers for thorough reading and comments that have improved the quality of the manuscript.

Authors' contributions
TL formulated the problem of this research work and interpreted and discussed the results. SA computed the results and did the major work in the writing of the manuscript. Both authors read and approved the final manuscript.

Funding
Not applicable.

Availability of data and materials
Not applicable.

Competing interests
The authors declared no potential conflicts of interest with respect to the research and authorship of this article.

Received: 17 April 2020 Accepted: 26 November 2020
Published online: 09 December 2020

References

1. Reddy, N.B., Maddileti, P., Reddy, S.B.: Combined impact of viscous dissipation, heat source and radiation on MHD flow past an exponentially stretching sheet with Soret and Dufour effects. Int. J. Innov. Technol. Exploring Eng. **9**(4), 342–347 (2020). https://doi.org/10.35940/ijitee.D1188.029420
2. Babu, R.S., Venkateswarlu, S., VLakshmi, J.K.: Effect of magnetic field and radiation on MHD heat and mass transfer of micropolar fluid over stretching sheet with Soret and Dufour effects. Int. J. Appl. Eng. Res. **13**(12), 10991–11000 (2018)

3. Sekhar, K.V.C., Manjula, V.: MHD slip flow of Casson fluid over an exponentially stretching inclined permeable sheet with Soret–Dufour effects. Int. J. Civil Eng. Technol. **9**(3), 400–417 (2018)
4. Reddy, N.A., Janardhan, K.: Soret and Dufour effects on MHD Casson fluid over a vertical plate in presence of chemical reaction and radiation. Int. J. Curr. Res. Rev. **9**(24), 55–61 (2017). https://doi.org/10.7324/IJARA.2017.92411
5. Gbadeyan, J.A., Oyekunle, T.L., Fasogbon, P.F., Abubakar, J.U.: Soret and Dufour effects on heat and mass transfer in chemically reacting MHD flow through a wavy channel. J. Taibah Univ. Sci. **12**(5), 631–651 (2018)
6. Parandhama, A., Raju, V.S., Raju, M.C.: MHD Casson fluid flow through a vertical plate. J. Comput. Appl. Res. Mech. Engi. **9**(2), 343–350 (2019). https://doi.org/10.22061/Jcarme.2019.4015.1476
7. Salawu, S.O., Dada, M.S.: Lie group analysis of Soret and Dufour effects on radiative inclined magnetic pressure-driven flow past a Darcy–Forchheimer medium. J. Serb. Soc. Comput. Mech. **12**(1), 108–125 (2018). https://doi.org/10.24874/jsscm.2018,12(01),pp.08
8. Iftikhar, N., Baleanu, D., Husnine, S.M., Shabbir, K.: Magnetohydrodynamic mixed convection flow of Jeffery fluid with thermophoresis, Soret and Dufour effects and convective condition. AIP Adv. **9**, 1–9 (2019). https://doi.org/10.1063/1.5086534
9. Sarada, K., Shanker, B.: The effects of Soret and Dufour on an unsteady MHD free convection flow past a vertical porous plate in the presence of suction or injection. Int. J. Eng. Sci. **2**(7), 13–25 (2013)
10. Kumar, M.B.: Free convective heat transfer in radiative MHD Casson fluid flow over a stretched surface of variable thickness. Chem. Process Eng. Res. **54**, 15–25 (2017)
11. Sumalatha, C., Shankar, B., Srinivasulu, T.: MHD stagnation point flow over a stretching sheet with the effects of thermal radiation and slip conditions. Int. J. Eng. Sci. Invent. **7**(3), 64–70 (2018)
12. Rajakumar, K.V.B., Balamurugan, K.S., Reddy, M.U., Murthy, C.V.R.: Radiation, dissipation and Dufour effects on MHD free convective Casson fluid flow through a vertical oscillatory porous plate with ion-slip current. Int. J. Heat Technol. **36**(2), 494–508 (2018). https://doi.org/10.18280/ijht.360214
13. Sreenivasulu, P., Poornima, T., Reddy, N.B.: Thermal radiation effects on MHD boundary layer slip flow past a permeable exponential stretching sheet in the presence of joule heating and viscous dissipation. J. Appl. Fluid Mech. **9**(1), 267–278 (2016). https://doi.org/10.18869/acadpub.jafm.68.224.20368
14. Agunbiade, S.A., Dada, M.S.: Effects of viscous dissipation on convective rotatory chemically reacting Rivlin–Ericksen flow past a porous vertical plate. J. Taibah Univ. Sci. **13**(1), 402–413 (2019). https://doi.org/10.1080/16583655.2019.1582149
15. Reddy, Y.S.K., Reddy, B.R.B.: Unsteady Magnetohyrdro Dynamic convective heat and mass transfer in a boundary layer slip past an inclined permeable surface in the presence of chemical reaction and thermal radiation. Int. Refereed J. Eng. Sci. **7**(2), 16–29 (2018)
16. Kumar, B., Srinivas, S.: Unsteady hydromagnetic flow of Eyring–Powell nanofluid over an inclined permeable stretching sheet with joule heating and thermal radiation. J. Appl. Comput. Mech. **6**(2), 259–270 (2020). https://doi.org/10.22055/JACM.2019.29520.1608
17. Ragavan, C., Munirathinam, S., Govindaraju, M., Abdul Hakeem, A.K., Ganga, B.: Elastic deformation and inclined magnetic field on entropy generation for Walter's Liquid B fluid over a stretching sheet. J. Appl. Math. Comput. Mech. **18**(2), 85–98 (2019). https://doi.org/10.17512/jamcm.2019.2.08
18. Reddy, P.B.A.: Magnetohydrodynamic flow of a Casson fluid over an exponentially inclined permeable stretching surface with thermal radiation and chemical reaction. Aim Shams Eng. J. (2016). https://doi.org/10.1016/j.asej.2015.12.010
19. Sharma, P.R., Choudhary, S.: Radiation and chemical reaction effects on unsteady slip flow over a semi infinite vertical porous plate embedded in a porous medium in the presence of inclined magnetic field. IJLTEMAS **3**(7), 17–24 (2014)
20. Olagunju, A.S., Joseph, F.L., Raji, M.T.: Comparative study of the effect of different collocation points on Legendre-Collocation methods of solving second-order boundary value problems. IOSR J. Math. **7**(2), 35–41 (2013)
21. Aysun, G., Salih, Y.: Legendre collocation method for solving nonlinear differential equations. Math. Comput. Appl. **18**(3), 521–530 (2013)

Publisher's Note
Springer Nature remains neutral with regard to jurisdictional claims in published maps and institutional affiliations.

Submit your manuscript to a SpringerOpen journal and benefit from:

► Convenient online submission
► Rigorous peer review
► Open access: articles freely available online
► High visibility within the field
► Retaining the copyright to your article

Submit your next manuscript at ► springeropen.com